UC Irvine

Title

Automatic three-dimensional segmentation combined with in vivo microvascular network imaging of human retina by intensity-based Doppler variance optical coherence tomography

Permalink

ISBN

Authors

Piao, Zhonglie
Huang, Shenghai
Qi, Li
et al.

Publication Date

DOI

Copyright Information

Peer reviewed

Automatic three-dimensional segmentation combined with in vivo microvascular network imaging of human retina by intensity-based Doppler variance optical coherence tomography

Zhonglie Piao[a,c], Shenghai Huang[a,b], Li Qi[a], Jiang Zhu[a], Fan Lu[b],
Zhongping Chen[a]

[a]Beckman Laser Institute, University of California, Irvine, Irvine, CA 92612, USA; [b]Wenzhou Medical University, School of Optometry and Ophthalmology, 270 Xueyuan Road, Wenzhou 325027, China; [c]Department of Cogno-Mechatronics Engineering, Pusan National University, Busan, 609-735, Korea

ABSTRACT

Optical coherence tomography (OCT) is a noninvasive method for retinal imaging. In this work, we present an *in vivo* human retinal microvascular network measurement by an intensity-based Doppler variance (IBDV) based on swept-source OCT. In addition, an automatic three-dimensional (3-D) segmentation method was used for segmenting intraretinal layers. The microvascular networks were divided into six layers by visualizing of each individual layer with enhanced imaging contrast. This method has potential for earlier diagnosis and precise monitoring in retinal vascular diseases.

Keywords: Optical coherence tomography; swept-source OCT; Doppler OCT; Doppler variance; intensity-based Doppler variance; retina; angiography; 3-D segmentation; dynamic programming

1. INTRODUCTION

The visualization of retinal vascular morphology allows earlier diagnosis and precise monitoring of several retinal diseases, such as diabetic retinopathy, retinal vascular occlusive disease, and choroidal neovascularization. In clinics, fundus fluorescein angiography is widely used as the gold standard for vascular imaging of retina and choroid. However, it is invasive and can only provide two-dimensional (2-D) imaging of the fundus.[1, 2]

Optical coherence tomography (OCT) is a noninvasive imaging modality with high-resolution which can provide three-dimensional (3-D) structural imaging of the macula and optic nerve head. Doppler OCT is a functional extension of OCT, which was developed for visualization and measurement of the blood flow in blood vessels.[3-5] Phase-resolved Doppler variance method was first investigated for mapping blood vessels.[6, 7] More recently, several amplitude variance methods, such as speckle variance,[8] correlation mapping, [9] split-spectrum amplitude-decorrelation angiography,[10] intensity-based Doppler variance (IBDV), [11-13] have been introduced for microvascular imaging. Compared with the phase-resolved method, the amplitude variance methods do not depend on phase stability. By employing the IBDV method, we successfully mapped the human choroidal blood vessel network in a phase instable situation.[11]

The vascular morphology of intraretinal layers can be obtained by combining OCT angiography with 3-D segmentation of intraretinal layers. Several segmentation methods have been successfully applied in 2-D segments of the intraretinal layer. The 3-D surfaces of the retina can be obtained by applying these 2-D based algorithms independently on each image. Compared with 2-D-based methods, 3-D-based segmentation methods can make full use of the information from neighboring B-scans and help improve the accuracy and robustness of the algorithm. A fast 3-D expansion of the dynamic programming method was demonstrated for vessel boundary detection on magnetic resonance imaging sequences with improved efficiency and robustness.[14]

Here, we report a method that combines the 3-D dynamic programming segmentation with IBDV based on swept-source OCT (SS-OCT) for visualizing microvascular morphology of intraretinal layers *in vivo* in normal and high myopia subjects. The microstructure network with the 3-D structure of the retina has potential for early diagnosis and precise monitoring in retinal vascular diseases.

*z2chen@uci.edu; phone 1 949 824-1247; fax 1 949 824-8413; http://octlab.eng.uci.edu

2. METHODS

The SS-OCT system used to acquire the OCT data is illustrated in Figure 1. The setup has been described in previous reports.[15, 16] A commercially available swept laser centered at 1050 nm with a 100-nm tuning range (Axsun Technologies, Inc, Billerica, MA, USA) was used. The wavelength sweeping speed was 100 kHz repetition rate with 50 % duty cycle. The laser was coupled to sample arm (20%) and reference arm (80%) by an 80/20 fiber coupler. The average power on the sample arm was measured as 1.8 mW. The light was scanned by an X-Y galvanometer scanner and guided in to the sample eye by a scan lens, a dichroic mirror and an eye lens. The dispersion of the ocular media was compensated by glass blocks in the reference arm. The interference fringes signal was digitized by a 500 MHz data acquisition board (ATS 9350, 12 bit, Alazar Technologies Inc., Pointe-Clarie, QC, Canada). We measured axial resolution as 6.4 μm and the imaging range as 3.0 mm at the retina. The signal-to-noise ratio (SNR) of the system was 95 dB and the 3-dB sensitivity of roll-off from imaging depth of 0.1 mm imaging to 1.5 mm was measured. Three right eyes (two normal subjects and one high myopia patient) were measured to demonstrate the feasibility of the method.
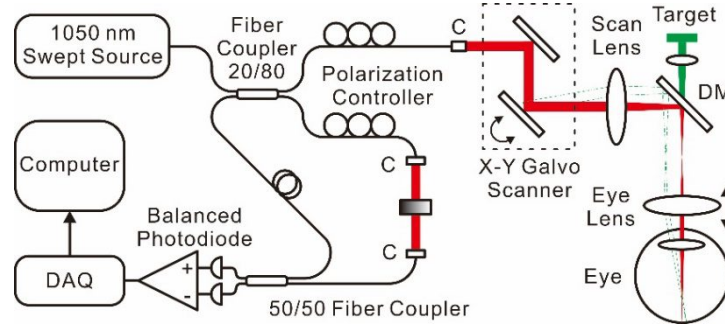

Figure 1. Schematic of the swept-source OCT system. C: collimator.

A custom-built data acquisition and processing software was developed with Microsoft C ++ 2012 with GPU computing acceleration. Each set of 3-D measurements was composed of 200 slices of 400 A-lines over an area of 2.5 mm × 2.5 mm. Each slice was composed of eight sequential B-scans at the same position. Figure 2 shows the flow diagram of the IBDV method combined with 3-D segmentation after obtaining the complex OCT data by preprocessing the interference signal.

The IBDV method was used to visualize the retinal microvascular network.[11] The time difference (T) was increased by using the interframe method. A subpixel registration algorithm was used to align sequential B-scans in both fast transverse direction x, and axial direction z. The variance value (σ^2) between sequential B-scans in the same position is given by[11]

$$\sigma^2 = \frac{1}{T^2}\left[1 - \frac{\sum_{m=1}^{M}\sum_{n=1}^{N-1}\left(|A_{n,m}||A_{n+1,m}|\right)}{\sum_{m=1}^{M}\sum_{n=1}^{N-1}\frac{1}{2}\left(|A_{n,m}|^2 + |A_{n+1,m}|^2\right)}\right]$$

(1)

where M is the number of the depth points that are averaged and N is the number of B-scans at the same position. The SNR can be increased by choosing larger Z, N. In this application, the M is the set at 2 and the N is the set at 8. $A_{n,m}$ denotes the amplitude value which is extracted from the complex OCT data. Finally, a threshold based on the histogram analysis of the averaged intensity images is used to remove the noise.

The boundaries of each layer were required to obtain the intraretinal layers. We used a 3-D expansion of the dynamic programming method for the automated boundaries detection. In the 2-D image, each pixel is treated as a node in the graph, and the links connecting the nodes are called edges. The values of the links are assigned based on the intensity of the pixels. The start node is a virtual node which connects to the nodes in the first column in the image and the weights are assigned to zero. Correspondingly, the end node is also a virtual node which connects to the nodes in the last column. The boundaries can be found by searching the minimum cost of the path from the start node to the end node. For the 3-D image, the surfaces of the layers were achieved by sequentially performing the search process in the fast scan plane and slow scan plane. The dynamic programming provides and efficient optimization method to find the minimum cost of the surface.

Consider a volumetric image $R_1(x, y, z)$ of size $X \times Y \times Z$, where the X and Y are the numbers of fast scan and slow scan, and Z denotes the depth. The iterative cost function in two directions is given by[14]

$$C_1(x, y, z) = \min_{-d_1 \leq i \leq d_1}\{C_1(x + i, y - 1, z) + w(x + i, x)\} \tag{2}$$

$$C_2(x, y, z) = \min_{-d_2 \leq i \leq d_2}\{C_2(x - i, y + j, z)\} + C_1(x, y, z) \tag{3}$$

for $1 < x \leq X$ and $1 < y \leq Y$, where C_1 and C_2 are the accumulation costs in the x-z plane, respectively. The initialization of C_1 and C_2 are assigned by $R(x, y, z)$. The parameters d_1 and d_2 constrain the searching range which can be used to control the smoothness of the surface. The volumetric image $R(x, y, z)$ is the intensity gradient image along the vertical direction. $w(x + i, x)$ denotes the weights from node $(x + i, y\text{-}1, z)$ to node (x, y, z) and the weights can be calculated as follows[17]

$$w(x + i, x) = 2 - r(x + i, y - 1, z) - r(x, y, z) + W_{min} \tag{4}$$

where $r(x, y, z)$ is the gradient value of the node (x, y, z) which is normalized to values between 0 and 1. The W_{min}, set at 1×10^{-5}, is the minimum weight for system stabilization.
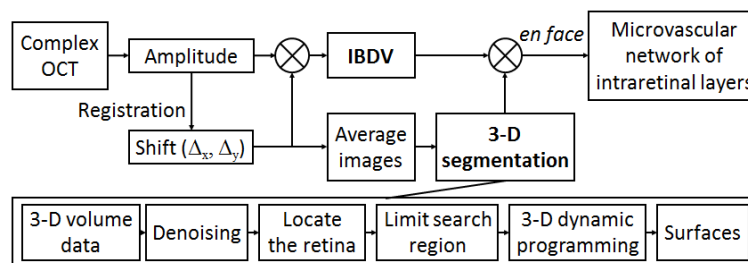

Figure 2. Flow diagram of intensity-based Doppler variance imaging process with 3-D segmentation.

The flow diagram of the IBDV with 3-D segmentation is shown in Figure 2. Eight consecutive B-scans were averaged after registration. A 3-D median filter was applied to the volumetric data using a window size of 5×3×5 voxels. The initial location of the retina could be obtained from the A-scan profile. It was determined by the inner limiting membrane (ILM, the first high reflective increase from the inner side of the retina) layer and retinal pigment epithelium (RPE, the highest peak after the ILM layer) layer. Finally, the surfaces of ILM, nerve fiber layer (NFL)/ganglion cell layer (GCL), inner plexiform layer (IPL)/inner nuclear layer (INL), INL/outer plexiform layer (OPL), OPL/outer nuclear layer (ONL), inner segment (IS)/ outer segment (OS), and RPE/choroid were detected by the automatic algorithm. Combined with the 3-D surfaces data, the volumetric microvascular signal of the retina could be segmented into different layers from the IBDV dataset. The *en face* projection view of the microvascular network for intraretinal layers was produced by using the maximum intensity projection (MIP) method.
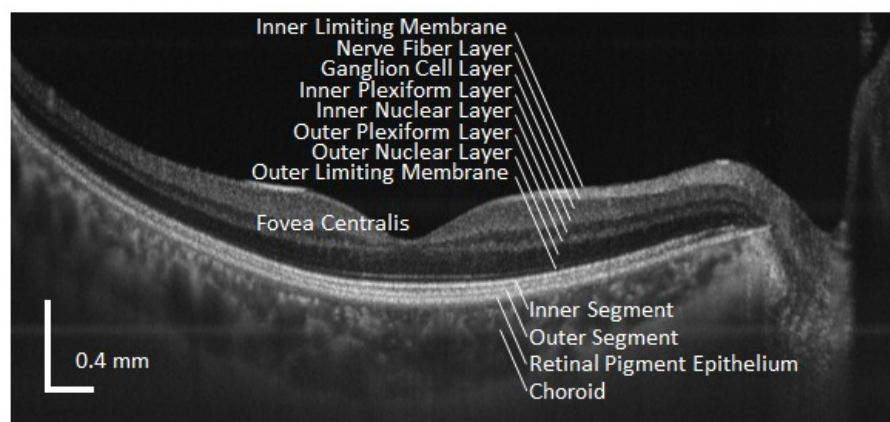

Figure 3. Wide-field 2-D image of macula and optic nerve head of a healthy right eye.

3. RESULTS

Three right eyes (two normal subjects and one high myopia patient) of volunteers were measured. A fixation target was used to control the location of the measurement. Figure 3 shows the 2-D wide-field image of macula and optic nerve head of a healthy eye. Eight B-scan images were averaged for increasing detection sensitivity and resolution. The total field of view is approximately 35 degrees. The 3-D segmentation of an imaging area of 2.5 mm × 2.5 mm is shown in Figure 4 (a). The retina from ILM layer to RPE/choroid boundary can be divided in to six layers, and seven surfaces of the intraretinal layers were segmented automatically by the algorithm [Figure 4 (b)]. The total processing time for extracting the surface was ~8 second, and the results were close to the manual segmentation.
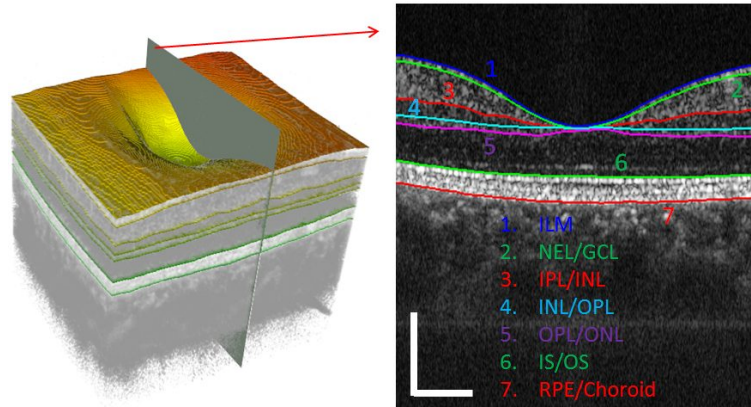

Figure 4. Three-dimensional segmentation of the retina. (a) 3-D rendering of the seven segmented surfaces from the ILM layer to the RPE-Choroid boundary. (b) The corresponding 2-D cross-section with segmented boundaries indicated by the plane in (a). Scale bar: 0.4 mm.

The right eyes of two normal subjects and one high myopia patient were imaged. The microvascular network of the macular retina was obtained by using the IBDV method. From cross-sectional OCT [Figures (a), (b)] and IBDV [Figure (c), (d)] images, most of the vessel signals were located in the inner retina and choroid. The signals in the outer retina should relate to the shadow artifact from the upper layers.
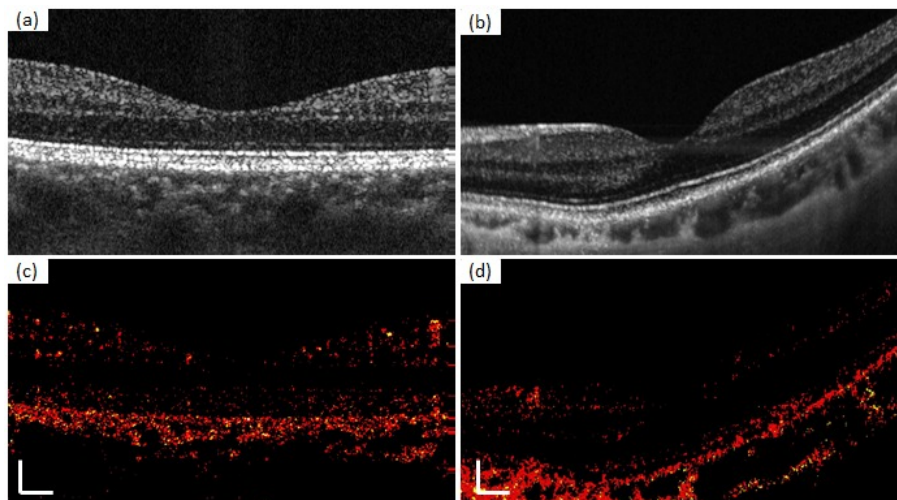

Figure 5. *In vivo* cross sectional OCT and IBDV images of (a), (c) healthy and (b) (d) high myopia subjects.

From the maximum intensity projection, the capillary network around the foveal avascular zone can clearly be visualized. The microvascular network of the macular retina was divided into six layers. In Figure 6 (a)-(f), we can see the *en face* MIP view of the microvascular network of the six layers: NFL, GCL+IPL, INL, OPL, ONL+IS, and OS+RPE. Most of the vessels are found in the inner retina which agrees with the known anatomy.
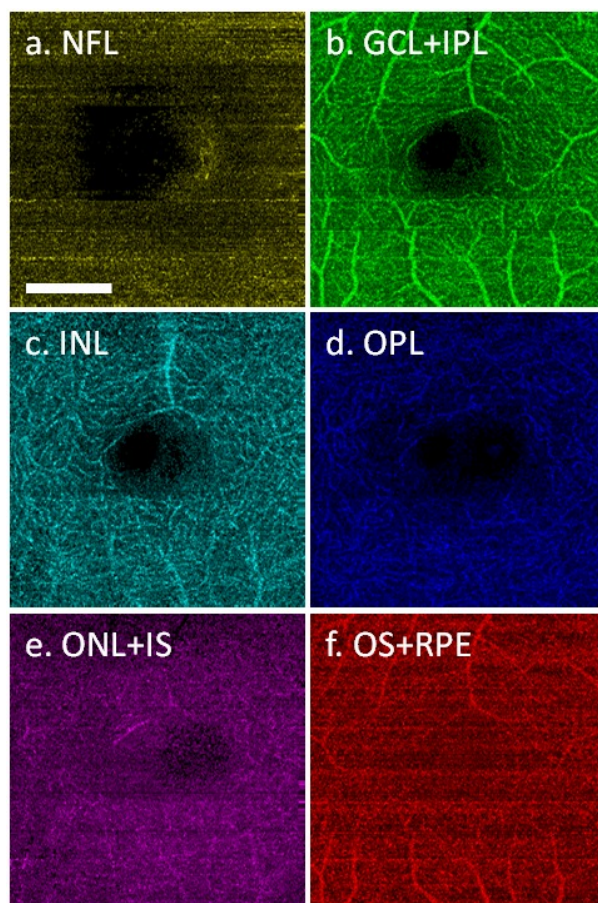
Figure 6. IBDV method combined with 3-D segmentation of the retina. *En face* MIP view of six individual layers: (a) NFL, (b) GCL+IPL, (c) INL, (d) OPL, (e) ONL+IS and (f) OS+ RPE. Scale bar: 0.5 mm.

4. CONCLUSION

We have demonstrated a 3-D segmentation combined with IBDV based on a SS-OCT system at 1050 nm. Using this method, three right eyes were imaged and 3-D data of the retina centered on the macula with 2.5 mm × 2.5 mm image area obtained. The seven surfaces of six layers were successfully segmented automatically, and microvascular networks on each layer were acquired. The morphology of the microvascular network for the individual intraretinal layers can be visualized, and the segmentation method can also be used to enhance contrast of the vascular images. This method has potential for earlier diagnosis and precise monitoring in retinal vascular diseases.

ACKNOWLEDGMENTS

REFERENCES

[1] Yannuzzi, L.A., Rohrer, K.T., Tindel, L.J., Sobel, R.S., Costanza, M.A., Shields, W. and Zang, E., "Fluorescein angiography complication survey." Ophthalmology 93, no. 5, 611-617. (1986)

[2] Mendis, K. R., Balaratnasingam, C., Yu, P., Barry, C. J., McAllister, I. L., Cringle, S. J., and Yu, D. Y., "Correlation of histologic and clinical images to determine the diagnostic value of fluorescein angiography for studying retinal capillary detail. " Invest. Ophthalmol. Vis. Sci., 51(11), 5864-5869 (2010).

[3] Chen, Z., Milner, T. E., Dave, D., and Nelson, J. S., "Optical Doppler tomographic imaging of fluid flow velocity in highly scattering media." Opt. Lett., 22(1), 64-66 (1997).

[4] Chen, Z., Milner, T. E., Srinivas, S., Wang, X., Malekafzali, A., van Gemert, M. J., & Nelson, J. S., "Noninvasive imaging of in vivo blood flow velocity using optical Doppler tomography. " Opt. Lett., 22(14), 1119-1121 (1997).

[5] Zhao, Y., Chen, Z., Saxer, C., Xiang, S., de Boer, J. F., and Nelson, J. S., "Phase-resolved optical coherence tomography and optical Doppler tomography for imaging blood flow in human skin with fast scanning speed and high velocity sensitivity. " Opt. Lett., 25(2), 114-116 (2000).

[6] Zhao, Y., Chen, Z., Saxer, C., Shen, Q., Xiang, S., de Boer, J. F., and Nelson, J. S., "Doppler standard deviation imaging for clinical monitoring of in vivo human skin blood flow. " Opt. Lett., 25(18), 1358-1360 (2000).

[7] Yu, L., Nguyen, E., Liu, G., Choi, B., & Chen, Z., "Spectral Doppler optical coherence tomography imaging of localized ischemic stroke in a mouse model. " J. Biomed. Opt., 15(6), 066006-066006. (2010).

[8] Mariampillai, A., Standish, B. A., Moriyama, E. H., Khurana, M., Munce, N. R., Leung, M. K., ... and Yang, V. X., "Speckle variance detection of microvasculature using swept-source optical coherence tomography. " Opt. Lett., 33(13), 1530-1532 (2008).

[9] Enfield, J., Jonathan, E., and Leahy, M., "In vivo imaging of the microcirculation of the volar forearm using correlation mapping optical coherence tomography (cmOCT). " Biomed. Opt. Express, 2(5), 1184-1193 (2011).

[10] Jia, Y., Tan, O., Tokayer, J., Potsaid, B., Wang, Y., Liu, J.J., Kraus, M.F., Subhash, H., Fujimoto, J.G., Hornegger, J. and Huang, D., "Split-spectrum amplitude-decorrelation angiography with optical coherence tomography. " Opt. Express, 20(4), 4710-4725 (2012).

[11] Liu, G., Chou, L., Jia, W., Qi, W., Choi, B. and Chen, Z., "Intensity-based modified Doppler variance algorithm: application to phase instable and phase stable optical coherence tomography systems." Opt. Express,19(12),11429-11440 (2011).

[12] Liu, G., Jia, W., Sun, V., Choi, B., and Chen, Z., "High-resolution imaging of microvasculature in human skin in-vivo with optical coherence tomography." Opt. express, 20(7), 7694-7705 (2012).

[13] Liu, G., Lin, A.J., Tromberg, B.J. and Chen, Z., "A comparison of Doppler optical coherence tomography methods." Biomed. Opt. Express, 3(10), 2669-2680 (2012).

[14] Cheng, D.C. and Lin, J.T., "Three-dimensional expansion of a dynamic programming method for boundary detection and its application to sequential magnetic resonance imaging (MRI)." Sensors, 12(5), 5195-5211 (2012).

[15] Potsaid, B., Baumann, B., Huang, D., Barry, S., Cable, A.E., Schuman, J.S., Duker, J.S. and Fujimoto, J.G., "Ultrahigh speed 1050nm swept source/Fourier domain OCT retinal and anterior segment imaging at 100,000 to 400,000 axial scans per second. " Opt. Express, 18(19), 20029-20048 (2010).

[16] Huang, S., Piao, Z., Zhu, J., Lu, F. and Chen, Z., "In vivo microvascular network imaging of the human retina combined with an automatic three-dimensional segmentation method." J. Biomed. Opt., 20(7), 076003-076003 (2015).

[17] Chiu, S.J., Li, X.T., Nicholas, P., Toth, C.A., Izatt, J.A. and Farsiu, S., "Automatic segmentation of seven retinal layers in SDOCT images congruent with expert manual segmentation." Opt. Express, 18(18), 19413-19428 (2010).